Wiley
Concepts in Magnetic Resonance: Part A
Volume 2026, Article ID 7473298, 12 pages
https://doi.org/10.1155/cmr/7473298

WILEY

Review Article

Erythrocyte Magnetics: Timescale of Alignment in NMR Spectrometers

Philip W. Kuchel,[1] **Stuart J. Elliott,**[2] **and Thomas R. Eykyn**[3]

[1]*School of Life and Environmental Sciences, University of Sydney, New South Wales 2006, Sydney, Australia*
[2]*Molecular Sciences Research Hub, Imperial College London, London W12 0BZ, UK*
[3]*School of Biomedical Engineering and Imaging Sciences, King's College London, St Thomas' Hospital, London SE1 7EH, UK*

Correspondence should be addressed to Philip W. Kuchel; philip.kuchel@sydney.edu.au

Received 12 August 2025; Revised 10 November 2025; Accepted 13 December 2025

Academic Editor: Michele Benedetti

Discocyte erythrocytes (red blood cells, RBCs) undergo spontaneous alignment in a uniform magnetic field, $\mathbf{B}_0$—a phenomenon initially observed via optical dispersion and light microscopy and later confirmed with nuclear magnetic resonance (NMR) spectroscopy. The phenomenon arises due to the diamagnetic anisotropy of membrane lipids and proteins, which have different energies when oriented parallel or perpendicular to the magnetic field. This behavior is directly relevant to modern NMR experiments performed on cells, in particular multiple quantum filtering of quadrupolar nuclei with nuclear spin quantum number $I > ½$, which are sensitive to the degree of alignment in intact cells and tissues, forming the basis of our present investigations. Using a quartic equation to represent the surface of a discocyte cell and the boundary element method to integrate over a triangular mesh, we compute the minimum-energy orientation of an RBC in $\mathbf{B}_0$. At a field strength of $\mathbf{B}_0 = 9.4$ T, the energy difference between parallel and orthogonal alignments was calculated to be ~1200 k_BT, the latter being Boltzmann's constant k_B times the absolute temperature T, which is the thermal energy of a single particle in solution. Using hydrodynamic theory, we estimate a characteristic realignment time (which has a theoretical $1/||\mathbf{B}_0||^2$ dependence) of ~300 ms at this field strength and extend this to consider the effects of collective behavior in densely packed RBC suspensions. Our findings agree with experimental data showing subsecond reorientational dynamics in strong magnetic fields and provide a physical framework for interpreting magnetic-field-induced structural order in biological tissues, which inform the development of new NMR and magnetic resonance imaging (MRI) methodologies for probing anisotropy, membrane architecture, and cellular organization in vivo.

Keywords: diamagnetic anisotropy; erythrocyte magnetization; magnetic alignment of cells; NMR of cells; red blood cells

1. Introduction

1.1. Aim and Rationale. Our goal is to establish a rigorous mathematical framework for calculating the reorientation time of an erythrocyte (red blood cell, RBC) when subjected to the strong magnetic field of a nuclear magnetic resonance (NMR) spectrometer or magnetic resonance imaging (MRI) scanner. As the analysis unfolds, it becomes clear that key experimental data, particularly the magnetic susceptibilities of membrane constituents, play a pivotal role in these calculations. In many respects, however, the available values remain incomplete. Should more accurate or revised data become available, the simulations (implemented in *Mathematica*) can readily be rerun to yield future updated predictions. We are confident that the underlying theoretical model is sufficiently robust to accommodate such refinements without compromising its general validity. Our calculated value for the reorientation time of an RBC is valid given the experimental data available.

1.2. Overview. The alignment of RBCs in strong, uniform magnetic fields is a striking and well-documented (although perhaps nonintuitive) biophysical phenomenon that has been explored through various experimental techniques over the past 60 years. The characteristic discoid shape of mammalian RBCs, excepting the ellipsoidal cells found in three genera of Camelidae, combined with the inherent diamagnetic anisotropy of the cell membrane, gives rise to a magnetic torque capable of aligning the cells almost completely, with their disk planes oriented parallel to the direction of the applied magnetic field.

1.3. Historical Pre-NMR Investigations. The earliest evidence for this magnetic alignment came from the work of Murayama in 1965 [1]. He reported magnet-induced birefringence under a light microscope in suspensions of RBCs from a donor with sickle cell anemia; the cells were aligned perpendicular to the direction of the magnetic field, consistent with the polymerization of the mutant hemoglobin. This original observation was significantly expanded in 1993 by Higashi and colleagues [2], who used laser light scattering to reveal the rapid, subsecond reorientation of RBCs in a high magnetic field, up to 8 T in a superconducting magnet. When RBCs were immobilized in gelatin during exposure to the magnetic field, nearly complete alignment of their disk planes parallel with the magnetic field vector $\mathbf{B}_0$ was observed. From these results, the researchers estimated an anisotropic diamagnetic susceptibility $\Delta\chi$ of 8×10^{-22} emu/RBC. This anisotropy was attributed to the membrane lipids rather than the cytoplasm, which being a viscous fluid was deemed to be unlikely to contribute significantly to the torque acting on the cell.

In a follow-up study, Higashi et al. examined glutaraldehyde-fixed RBCs [3]. Contrary to expectations that such cells, now effectively rigid disks, would align with their disk planes parallel to $\mathbf{B}_0$, the cells instead aligned orthogonal to the field. This counterintuitive result was explained by the effect of the chemical fixation, which had converted the hemoglobin to paramagnetic Fe(III)-containing methemoglobin and implied that some of the hemoglobin molecules had become bound to the membrane, thus exerting a torque. As a result, the minimum-energy orientation was obtained with the disk planes perpendicular to $\mathbf{B}_0$, consistent with the induced paramagnetic contribution.

Further studies in Japan by Suda and Uneo [4] aimed to disentangle the respective contributions of the plasma membrane and hemoglobin to RBC magnetic orientation. Their 1994 work measured changes in the electrical resistivity of buffer solutions containing either intact RBCs or membrane "ghosts" when exposed to a magnetic field. Subsequent experiments [5] revealed that electrical resistivity decreased when the magnetic field was applied parallel to the electric field, supporting the presence of anisotropic magnetic effects. However, the diamagnetic anisotropy they inferred ($\Delta\chi\approx8\times10^{-28}$ emu/RBC) was markedly smaller than the previously reported values.

This notable discrepancy in reported susceptibility values underscored the need for a more direct and reliable approach. Thus, our work turned to a method grounded in NMR spectroscopy, enabling precise measurements of RBC orientation and simultaneous biochemical and biophysical responses, without removing the cell sample from the bore of the superconducting magnet.

1.4. Historical NMR. By 1991 [6], it had been demonstrated that protein diffusion within RBCs is subject to intracellular restriction when compared with hemolysates. Numerical simulations soon followed [7], predicting that structured suspensions would give rise to exaggerated, diffraction-like signals in pulsed field-gradient spin-echo (PGSE) NMR experiments, the so-called q-space plots [8]. This led to the first experimental demonstration of the diffusion–diffraction phenomenon in a biological (cellular) sample, using suspensions of RBCs [9]. The spatial coherence revealed in the q-space plots strongly suggested that the sample exhibited extensive order. The most plausible explanation, subsequently verified, was that the RBCs had become aligned with their disk planes parallel to the magnetic field.

Figure 1(a) shows a typical q-space plot from a PGSE experiment on RBC suspensions with different hematocrit (*Ht*) values, acquired on a 9.4 T spectrometer capable of delivering a maximum gradient amplitude of 9.8 $\mathrm{T\,m^{-1}}$, revealing distinct "diffusion coherence"—multislit interference, and single slit diffraction analogs of optical counterparts. Diffraction minima appear at q values that reflect the average inverse diameter of the aligned cells, which is 6.2 μm for a biconcave disk with a diameter of 8 μm aligned parallel to the magnetic field.

Further work consolidated this interpretation. Specific q-space features were assigned to particular restricted diffusion geometries reflecting erythrocyte morphology [11]. Additional NMR confirmation came from diffusion tensor analysis, which revealed anisotropic water diffusion in RBC suspensions [12]. Theoretical modeling added more depth: Regan et al. developed simulations of molecular diffusion in packed-cell lattices [13], taking into account packing geometry, membrane permeability, and alignment effects on q-space NMR data.

More recently, Protopapas et al. proposed a theoretical model for mapping the internal magnetic field of an RBC [14]. However, despite the title of their article, their analysis does not incorporate the concept of diamagnetic anisotropy of the membrane or field-induced alignment. In addition, the geometry of their RBC model diverges substantially from the actual shape of the human discocyte (see below), so it does not have direct bearing on the current analysis.

Taken together, our NMR studies compellingly established the alignment of RBCs in the strong magnetic field of NMR spectrometers. The primary mechanism was concluded to be the diamagnetic anisotropy of the membrane lipids, and this alignment leads to observable anisotropy in water diffusion. Such effects, captured in q-space plots derived from PGSE experiments, provide valuable insights into

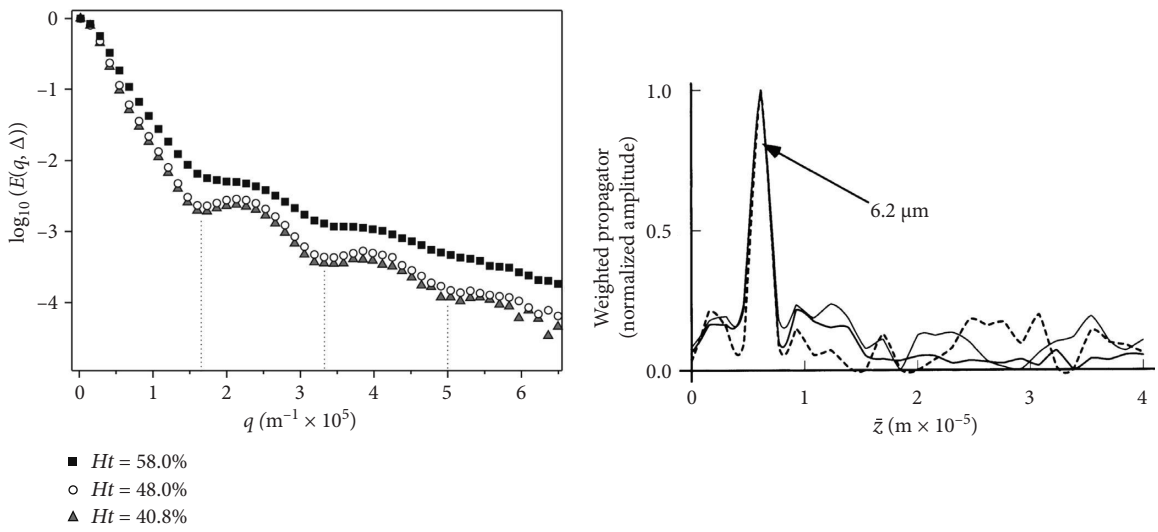

(a) (b)

FIGURE 1: (a) ^{1}H NMR q-space plots of the water signal from a suspension of human RBCs at different Ht values. The three diffraction minima (vertical dashed lines) result from water diffusing within the cells and appear at q values corresponding to the mean restricted diffusion distance. (b) Fourier transform of the second derivative of the q-space data yields a weighted propagator and a mean distance of 6.2 μm, corresponding to the average distance across an RBC with a diameter of 8 μm aligned parallel to the direction of the z diffusion gradient and therefore also parallel to the magnetic field $\mathbf{B}_0$. The details of the experimental setup are provided in the primary references. (Adapted with permission from Ref. [10]).

the morphology and biophysical behavior of RBCs in high Ht suspensions.

Given the ease and reliability of implementing rapid diffusion (hence shape) measuring q-space NMR methods that are applicable to studying RBC alignment [15, 16], we sought to place these observations on a firm physical and chemical foundation. Our objective here was to calculate the magnetic energy difference between two orientations of a human RBC in a uniform magnetic field, $\mathbf{B}_0$—one with the disk planes perpendicular to the field and the other with them parallel. This analysis would determine whether the alignment was complete or only partial across the RBC ensemble and allow an estimation of the timescale for the reorientation.

To set the stage for these calculations, we begin by invoking key concepts from magnetostatics [17, 18], and to emphasize the consistency of the physical units used, they are given in detail for the first few equations.

2. Theory

2.1. Basic Physical Equations. The Maxwell equations for a magnetostatic system are [17, 18]

$$\nabla.\mathbf{B} = 0, \tag{1}$$

$$\nabla \times \mathbf{H} = 0, \tag{2}$$

where SI units are used throughout, $\mathbf{B}$ is the magnetic induction (units: $\mathrm{N\,m^{-1}\ A^{-1}}$), and $\mathbf{H}$ is the magnetic field strength ($\mathrm{A\,m^{-1}}$)—in less formal discussions, these terms are often used interchangeably, but for the sake of evolving rigorous magnetic theory, it is worth adhering to the correct terminology. A key constitutive relation (viz., a mathematical relationship between variables that describe a given physical phenomenon) is

$$\mathbf{B} = \mu_0(\mathbf{H} + \mathbf{M}), \tag{3}$$

where $\mu_0 = 4\pi \times 10^{-7}\ \mathrm{H\,m^{-1}}$ ($\mathrm{V\ (A\ s^{-1})^{-1} m^{-1} = J\,C^{-2}\,m^{-1}} \equiv \mathrm{N\,C^{-2}}$) is the magnetic permeability of free space and the magnetization $\mathbf{M}$, which is the magnetic dipole moment per unit volume (units: $\mathrm{A\,m^2\ m^{-3} = A\,m^{-1}}$), is given by

$$\mathbf{M} = \chi\mathbf{H}. \tag{4}$$

Noting that the magnetic susceptibility χ is dimensionless, then

$$\mathbf{B} = \mu_0(1 + \chi)\mathbf{H} = \mu\,\mathbf{H}, \tag{5}$$

where $\mu = \mu_0\ (1 + \chi)$ is the permeability of the medium. The factor

$$\frac{\mu}{\mu_0} = (1 + \chi), \tag{6}$$

is the relative magnetic permeability of the medium.

2.2. Magnetic Susceptibility. All materials with paired electrons are diamagnetic, which means that when subjected to a magnetic field, they develop their own field that opposes the main one. This feature is characterized by a magnetic susceptibility $\chi < 0$, meaning that their magnetic permeability μ is (slightly) less than that of free space ($\mu < \mu_0$). In contrast, paramagnetic substances with unpaired electrons have $\chi > 0$, resulting in $\mu > \mu_0$. While all materials exhibit at least weak diamagnetism, many are also paramagnetic, and

a select few are ferromagnetic. An interesting case is molecular oxygen (O_2), which is paramagnetic due to its triplet ground state, while oxyhemoglobin is diamagnetic and deoxyhemoglobin is paramagnetic, reflecting the low or high spin complexes of Fe. Transition metal ions generally exhibit paramagnetism, while Group 1 and Group 2 cations (*e.g.*, Li^+, Na^+, K^+, Ca^{2+}, and Mg^{2+}) are all diamagnetic. Typically, paramagnetism is stronger than diamagnetism at room temperature, but it decreases with increasing temperature. The Curie temperature denotes the point at which a ferromagnetic material loses its ferromagnetism and becomes paramagnetic.

To give context, Table 1 lists representative volume magnetic susceptibilities for several biologically significant substances, including water and various fatty acids. These values are adapted from experimental data [20]. For the calculations presented in this study, it is the volume magnetic susceptibility that is required, since it is the volume, not the molar mass, that governs how a substance contributes to the bulk magnetic properties of the RBC membrane. This distinction is crucial when characterizing the membrane's response to an external magnetic field. To proceed toward defining the magnetic energy of the system—namely, an RBC in a uniform magnetic field—we need to first establish a precise mathematical representation of the RBC's shape.

2.3. Mathematical Description of RBC Shape–Disk-Cyclide Model. Several precursor models lack a sufficient number of parameters to yield the correct form of the distinctive biconcave shape of an RBC. On the other hand, a quartic equation provides good correspondence between theoretical predictions and microscope images of RBCs [21],

$$\left(x^2 + y^2 + z^2\right)^2 + P\left(x^2 + y^2\right) + Q z^2 + R = 0. \tag{7}$$

The principal dimensions of an RBC are its main diameter, $d = 8.0\,\mu m$; its central (between the dimples) thickness, $b = 1.0\,\mu m$; and its maximum thickness near the rim, $h = 2.12\,\mu m$. The analytical challenge, therefore, lies in relating these physical dimensions to the coefficients in equation (7). The resulting expressions are [21, 22]

$$P = -\frac{d^2}{2} + \frac{h^2}{2}\left(\frac{d^2}{b^2} - 1\right) - \frac{h^2}{2}\left(\frac{d^2}{b^2} - 1\right)\left(1 - \frac{b^2}{h^2}\right)^{(1/2)}, \tag{8}$$

$$Q = \frac{d^2}{b^2}P + \frac{b^2}{4}\left(\frac{d^4}{b^4} - 1\right), \tag{9}$$

$$R = -\frac{d^2}{4}P - \frac{d^4}{16}. \tag{10}$$

This shape is notably a coordinate surface in the disk-cyclide coordinate system as described by Moon and Spencer in their "*Field Theory Handbook*" [23]. Thus, the coordinate transformation equations cited there constitute three parametric equations that describe the shape of an RBC,

Table 1: Magnetic susceptibilities of substances commonly encountered in biological systems or experiments on them.

Compound name	χ (-10^6 SI units; dimensionless)[a] 20°C
Acetone	5.78
Benzene	7.68
Carbon tetrachloride	8.68
Dimethyl sulfoxide	8.55
D_2O	8.82
Ethanol	7.23
Ethylene glycol	8.77
D-Glucose	10.92 (25°C)
Glycerol	9.79
H_2O	9.04
Mannitol	11.4
Methanol	6.66
Myristic acid	8.31 (60°C)
Oleic acid	8.31 (18°C)
Palmitic acid	8.31 (62°C)
Toluene	7.76

[a]Reproduced from [19] with permission.

$$x = \frac{a}{\Lambda}\,\mathrm{cn}[\mu, k]\,\mathrm{cn}\left[\nu, k'\right]\cos[\psi], \tag{11}$$

$$y = \frac{a}{\Lambda}\,\mathrm{cn}[\mu, k]\,\mathrm{cn}\left[\nu, k'\right]\sin[\psi], \tag{12}$$

$$z = \frac{a}{\Lambda}\,\mathrm{sn}[\mu, k]\,\mathrm{dn}[\mu, k]\,\mathrm{sn}\left[\nu, k'\right]\,\mathrm{dn}\left[\nu, k'\right], \tag{13}$$

where sn, cn, and dn are the elliptic functions with elliptic modulus k, and $k' = \sqrt{(1-k^2)}$; the variables are μ, ν, and ψ, for which the domains of these independent variables are

$$0 \le \mu \le K, 0 \le \nu \le K', \text{ and } 0 \le \psi < 2\pi. \tag{14}$$

There are well-defined relationships between a, k, and μ_s (the special value of μ that determines the location of the RBC's maximum thickness), which then means that the parametric equations can also be used in *Mathematica*'s ParametricPlot3D to render the surface; see the Supporting Information for more details. This approach and the coordinate transformation relationships are not directly used here, but they provide the means for deriving analytical solutions of the magnetic field in and around an RBC. (Should they be needed for other work, they can be found in the primary references [21, 22].)

Variations of equations (7)–(10) have been proposed, including by Evans and Fung [24], and Philp [25], but these involve square roots mixed with integer-power terms. Our preference is for the formulation of equations (7)–(10) as it involves only integer powers of the independent variables, and it transitions seamlessly into the disk-cyclide coordinate system [23] with the alternative representation as three parametric (coordinate transformation) equations (see Supporting Information available here).

Next, we combine the shape of the RBC with the diamagnetic properties of the membrane constituents.

2.4. Magnetic Susceptibility Tensor. Fatty acid chains in phospholipid bilayers exhibit anisotropic diamagnetism due to their linear hydrocarbon structure. The electronic polarizability is greater perpendicular to the chain axis (imagine looking along the string of carbon atoms that are decorated with hydrogen atoms), enabling stronger induced electron currents circumferential to the carbon backbone under an external magnetic field. According to Lenz's law, a molecule's thermally driven motion excites electron currents whose direction is such as to oppose the molecule's motion in the magnetic field. As a result, the diamagnetic susceptibility measured along the chain axis ($\chi_{\parallel}$) is more negative than perpendicular to it ($\chi_{\perp}$). In other words, for fatty acid chains, the induced currents are strongly perpendicular to the chain axis (due to higher polarizability). Aligning the chain axis parallel to the magnetic field results in a stronger opposing moment and thus a higher magnetic energy. Hence, the minimum-energy configuration is achieved when the chain axis is perpendicular to the field, reducing the induced opposing moment. Consequently, lipid membranes tend to align with their plane parallel to the magnetic field, meaning that the fatty acid chains are perpendicular to it.

This outcome is common for aliphatic chains and other anisotropic molecules (*e.g.*, benzene rings and nucleic acid bases). Therefore, if the long molecular axis of the molecule is aligned with the uniform magnetic field's z-direction, and the tensor describing this property is ordered (χ_{11}, χ_{22}, χ_{33}), then χ_{33} ($\parallel$) is more negative than χ_{11} and χ_{22} ($\perp$). Equations (3) and (4) are central to determining the magnitude of the magnetization induced in the RBC membrane. It is also important to note that the magnetic susceptibility of the membrane lipids (such as palmitic, oleic, and stearic acid chains in phospholipids) χ_m is typically $\ll -10^{-6}$. Thus, we obtain

$$\mathbf{M} \cong \frac{\chi_m}{\mu_0}\mathbf{B}. \tag{15}$$

Equation (15) applies generally to anisotropic materials with small but tensorial magnetic susceptibility. For a membrane bilayer in RBCs oriented parallel to the x, y plane, equation (15) can be expressed as

$$\begin{pmatrix} M'_x \\ M'_y \\ M'_z \end{pmatrix} = \frac{1}{\mu_0}\begin{pmatrix} \chi_{\perp\mathrm{Memb}} & 0 & 0 \\ 0 & \chi_{\perp\mathrm{Memb}} & 0 \\ 0 & 0 & \chi_{\parallel\mathrm{Memb}} \end{pmatrix}\begin{pmatrix} B'_x \\ B'_y \\ B'_z \end{pmatrix}. \tag{16}$$

Here, $\chi_{\perp\mathrm{Memb}}$ is the magnetic susceptibility of the RBC membrane when it lies perpendicular to the main magnetic field. However, because the hydrocarbon chains of the membrane lipids lie perpendicular to the membrane surface, the magnetic susceptibility that applies is $\chi_{\parallel Lipid}$. Conversely, across the axis of a hydrocarbon chain, the induced diamagnetism is smaller ($\chi_{\perp\mathrm{Lipid}}$ is less negative), and again because the chains are aligned perpendicular to the membrane surface, $\chi_{\perp\mathrm{Lipid}}$ is the susceptibility of the membrane when the membrane surface is parallel to the magnetic field. In symbols, $\chi_{\parallel\mathrm{Lipid}} < \chi_{\perp\mathrm{Lipid}}$ (the former is more negative), while $\chi_{\parallel\mathrm{Memb}} > \chi_{\perp\mathrm{Memb}}$ (the latter is more negative). The primes in equation (16) indicate that the vectors are expressed in the membrane's local frame of reference.

2.5. Estimation of Diamagnetic Anisotropy. The RBC membrane is composed of approximately 50% lipids by mass, primarily cholesterol and phospholipids, with the remaining mass/volume made up of myriad different proteins. While most proteins are also diamagnetic, their diverse composition makes it difficult to assign a precise value to their contribution to the overall magnetic susceptibility; only an average estimate can be made. Calculations carried out for membrane proteins with known structures yield values of the volume diamagnetic anisotropy that are of similar orders of magnitude to those of lipids [26].

Therefore, in the following calculations, we focus on phospholipids with their fatty acid chains. The anisotropy of fatty acids is typically approximated by

$$\chi_{\parallel} = \chi_{\mathrm{avg}} + \frac{1}{3}\Delta\chi, \tag{17}$$

$$\chi_{\perp} = \chi_{\mathrm{avg}} - \frac{1}{6}\Delta\chi. \tag{18}$$

Derived from the traceless condition that

$$\chi_{\mathrm{avg}} = \frac{1}{3}\left(\chi_{\parallel} + 2\chi_{\perp}\right). \tag{19}$$

The values in Table 1 are these averages. A problem arises in the literature from the disparate choice of units and nonadherence to SI conventions; however, a useful conversion is 1 cgs unit = $4\pi \times 10^{-6}$ SI units. It is still impossible to obtain a consistent suite of values for the diamagnetic anisotropy of RBC membrane components. What is clear though, for many linear organic molecules, is that the diamagnetic anisotropy is ~10–15% of the average value. The volume magnetic susceptibility used in the following calculations was that of myristic, oleic, and palmitic acid, and 14% of this value gives $\Delta\chi = -1.13 \times 10^{-6}$. These values were then used in the attached *Mathematica* Notebook—see the Supporting Information for more details. The justification of $\Delta\chi$ ~14% is convoluted. It is a value that can be inferred from the work of Seelig [27, 28] based on Pauling's [29] molecular orbital reasoning and Lonsdale's [30] classical study, which then can be linked to that of Higashi [2]. For our current purposes, its "reasonableness" was accepted [25].

2.6. Minimum-Energy Configuration. A fundamental thermodynamic proposition is that at equilibrium, an RBC will be oriented in a uniform magnetic field $\mathbf{B}_0$ such that its total induced magnetization is minimized. Since the magnetic susceptibility of the phospholipids is negative, the configuration that minimizes energy is the one where the majority of the area of the RBC membrane lies parallel to $\mathbf{B}_0$ and the lipids lie perpendicular. To quantify this effect, we must calculate the interaction energy (U) between $\mathbf{B}_0$ and the

membrane's *induced* magnetization **M**, noting that the RBC has a closed surface with its various orientations with respect to $\mathbf{B}_0$. Therefore, the energy is given by the integral over the whole volume V of the RBC membrane [18],

$$U = -\frac{1}{2}\int_V \mathbf{M}.\mathbf{B}\, dV. \tag{20}$$

The factor of ½ in equation (19) warrants explanation, as follows: We imagine that **M** builds up from 0 to **M** as the body is moved into $\mathbf{B}_0$, which works against this insertion. At each stage, the instantaneous magnetization is $\lambda\mathbf{M}$ ($\lambda \epsilon [0, 1]$), so the increment of work (energy) is

$$dU = -\mathbf{B_0} \cdot \lambda\mathbf{M}\, d\lambda. \tag{21}$$

Hence, the total work (energy) is given by the integral

$$U = -\int_0^1 \mathbf{B}_0 \cdot \lambda\mathbf{M}\, d\lambda = -\frac{1}{2}\mathbf{B}_0 \cdot \mathbf{M}. \tag{22}$$

This result pertains to each unit volume, so to calculate the total energy, the integral is taken over the whole volume, as given in equation (22). In other words, U is the magnetic potential energy stored in the object when placed in the magnetic field. The complementary part of the energy resides in the magnetic field itself, arising from the distortion of the external field due to the presence of the magnetized medium. Together, these contributions account for the total field energy of the system.

Placing a membrane in a previously uniform magnetic field perturbs this field, so strictly the value of **B** that applies in equations (16) and (22) is not the same as $\mathbf{B}_0$. However, since the perturbation is negligible (of the order of parts per million), mathematically it can be neglected. Specifically, the terms B'_x, B'_y, and B'_z in equation (16) are approximated by B'_{0x}, B'_{0y}, and B'_{0z}, respectively, and we therefore retain the factor of ½ in the expression for U (equation (22)).

2.7. Evaluating the Integral in Equation (22). There are two main numerical methods for solving partial differential equations with boundary conditions defined over a given domain like the RBC—the finite element method (FEM) and the boundary element method (BEM). The FEM involves discretizing the entire volume of the domain, while the BEM only requires meshing the surface of it. Because of *Mathematica's* ability to generate high-quality triangular meshes on surfaces, it is straightforward to approximate the integral in equation (22) to any desired level of accuracy by adjusting the mesh resolution. This advantage led us to choose the BEM approach. In practice, estimating U involves evaluating equation (22) by summing the energy contributions of each triangle weighted by its area and membrane thickness. The process is both time-efficient and scalable.

Figure 2 shows such a triangulation of an RBC surface using *Mathematica*'s function BoundaryDiscretizationRegion. Because the mesh triangles have various orientations relative to the main plane of the RBC, the magnetic susceptibility tensor must be transformed into each triangle's local coordinate

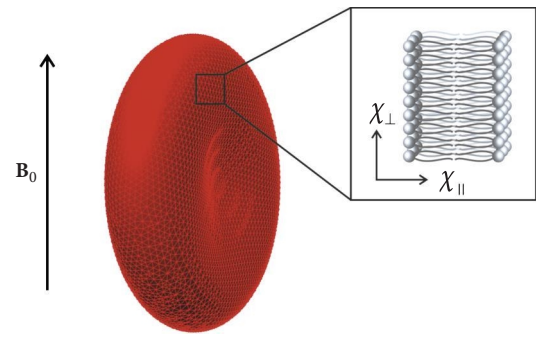

FIGURE 2: Triangulation/triangularization of the surface of an RBC represented by equations (7)–(10) in *Mathematica*. For illustration, the cell is oriented parallel to the magnetic field. Also shown is an illustration of the orientation of the lipids in the phospholipid bilayer annotated with the magnetic susceptibilities parallel $\chi_\parallel$ and perpendicular $\chi_\perp$ to the aliphatic chains.

system. To achieve this, we assume that the RBC is centered in a Cartesian coordinate system, lying in the *x,y*-plane. The external magnetic field $\mathbf{B}_0$ is initially aligned along the *z*-axis; however, changes in the orientation of the RBC relative to $\mathbf{B}_0$ can be modeled by performing the reverse of this and changing the direction of $\mathbf{B}_0$ relative to the RBC lying in the *x,y*-plane. This transformation is described by

$$\mathbf{B}_0 = B_{0,z}\,(\hat{j}\sin\alpha + \hat{k}\cos\alpha) = B_{0,z}\begin{pmatrix} 0 \\ \sin\alpha \\ \cos\alpha \end{pmatrix}, \tag{23}$$

where $B_{0,x}$, $B_{0,y} = 0$ and α is the angle of rotation of $\mathbf{B}_0$ around the *x*-axis. In other words, the symmetry of this problem means that this rotation of $\mathbf{B}_0$ is equivalent to rotating the RBC through the negative of this angle about the *x*-axis.

2.8. Coordinate Transformation Matrix. The following insight is required to correctly transform the magnetic susceptibility tensor to the Cartesian frame of reference in each mesh triangle [31]. Suppose that a matrix **A** operates on a vector **f** to yield a vector **g**,

$$\mathbf{g} = \mathbf{A}\mathbf{f}. \tag{24}$$

If the original coordinate system is transformed (rotated) by a matrix **R**, the components of **g** are now defined by

$$\mathbf{R}\,\mathbf{g} = \mathbf{R}\,\mathbf{A}\,\mathbf{f}. \tag{25}$$

This equality is undisturbed by inserting the identity matrix ($\mathbf{R^{-1}R} = \mathbf{I}$) into it,

$$\mathbf{R}\,\mathbf{g} = \mathbf{R}\,\mathbf{A}\left(\mathbf{R}^{-1}\,\mathbf{R}\right)\mathbf{f} = \left(\mathbf{R}\,\mathbf{A}\,\mathbf{R}^{-1}\right)\mathbf{R}\,\mathbf{f}. \tag{26}$$

By noting that $\mathbf{R}\ \mathbf{f}$ is simply **f** expressed in the new (transformed) coordinate system, we can view the composite matrix operator $\mathbf{R}\,\mathbf{A}\,\mathbf{R}^{-1}$ as that which acts on **g** to express it in the new coordinates. In other words, $\mathbf{R}\,\mathbf{A}\,\mathbf{R}^{-1}$ is the form taken by matrix **A** when it is transformed to the new axes, namely,

$$\mathbf{A}' = \mathbf{R}\,\mathbf{A}\,\mathbf{R}^{-1}. \tag{27}$$

2.9. Transforming the Magnetic Susceptibility Tensor. The mechanics of doing this transformation are as follows: Consider a mesh triangle with vertices v_1, v_2, and v_3 with coordinates (v_{1x}, v_{1y}, v_{1z}), (v_{2x}, v_{2y}, v_{2z}), and (v_{3x}, v_{3y}, v_{3z}), respectively, as represented in Figure 3. The three sets of coordinates define the tips of *position vectors* with all their tails at the origin, with their vector status denoted by using bold font style. The vectors that define the *edges* of the mesh triangle are given by $\mathbf{v}_2$-$\mathbf{v}_1$, $\mathbf{v}_3$-$\mathbf{v}_2$, and $\mathbf{v}_1$-$\mathbf{v}_3$, where, for example, the coefficients of the first difference vectors are (v_{2x}-v_{1x}, v_{2y}-v_{1y}, and v_{2z}-v_{1z}) and similarly for the other two.

From coordinate geometry, the normal vector $\mathbf{n}$ of the mesh triangle is given by the cross product of two edge vectors, calculated using the right-hand rule (anticlockwise) for naming the vertices (Figure 3),

$$\mathbf{n} = (\mathbf{v}_2 - \mathbf{v}_1) \times (\mathbf{v}_1 - \mathbf{v}_3). \tag{28}$$

To translate the normal vector to the origin of the Cartesian coordinate system, we normalize it. Thus,

$$\hat{\mathbf{n}} = \frac{(\mathbf{v}_2 - \mathbf{v}_1) \times (\mathbf{v}_1 - \mathbf{v}_3)}{\left|\left|(\mathbf{v}_2 - \mathbf{v}_1) \times (\mathbf{v}_1 - \mathbf{v}_3)\right|\right|}, \tag{29}$$

where the double bars denote the magnitude of the vector. The area dA of the mesh triangle is given by half the norm of the cross product of two of the edge vectors,

$$dA = \frac{1}{2}\left|\left|(\mathbf{v}_2 - \mathbf{v}_1) \times (\mathbf{v}_1 - \mathbf{v}_3)\right|\right|. \tag{30}$$

This value is then used when generating the weighted sum of energies over all mesh triangles, thus evaluating equation (22) (see below). The next step is to transform the magnetic susceptibility tensor in the laboratory frame of reference to the local frame of the mesh triangle. The angle made by $\hat{\mathbf{n}}$ (equation (31)) to the axes in the laboratory frame of reference is useful to have on hand in the analysis (see Figure 3),

$$\psi = \frac{\arctan x}{y}\left(\frac{\text{first element of } \hat{\mathbf{n}}}{\text{second element of } \hat{\mathbf{n}}}, \text{ gives rotation about } z - \text{axis}\right), \tag{31}$$

$$\theta = \arccos z\,(\text{third element of } \hat{\mathbf{n}}). \tag{32}$$

At this point, we might be tempted to employ the three Euler rotation matrices to transform from the fixed Cartesian coordinate frame, but it turns out that the approach using these matrices is plagued by potential numerical errors.

2.10. Rodrigues' Formula. In view of the previous reservations, Rodrigues' formula [32] was used to rotate the magnetic susceptibility tensor to align it with the normal vector of each corresponding mesh triangle. The formula rotates the vector $\hat{\mathbf{k}}$ through the angle θ about the normalized-normal vector to the plane containing $\hat{\mathbf{k}}$ and $\hat{\mathbf{n}}$ viz., $\hat{\mathbf{v}}$,

$$\hat{\mathbf{k}}_{\text{rot}} = \hat{\mathbf{k}}\cos\theta + (\hat{\mathbf{v}} \times \hat{\mathbf{k}})\sin\theta + \hat{\mathbf{v}}\,(\hat{\mathbf{v}} \cdot \hat{\mathbf{k}})\,(1 - \cos\theta), \tag{33}$$

where $\times$ and $\cdot$ denote the cross and scalar products for vectors. Importantly, equation (33) can be couched in terms of matrices [32], making implementation in *Mathematica* straightforward,

$$\mathbf{R} = \mathbf{I} + \sin\theta\,\mathbf{V} + \cos\theta\,\mathbf{V}^2, \tag{34}$$

where $\mathbf{V}$ is the skew-symmetric matrix (also denoted $[\mathbf{v}]_\times$) of *any* vector $\mathbf{v}$, with its Cartesian elements,

$$\mathbf{V} = \begin{bmatrix} 0 & v_{-z} & v_y \\ v_z & 0 & v_x \\ v_{-y} & v_{-x} & 0 \end{bmatrix}. \tag{35}$$

Hence, the operation of carrying out the vector cross product between *any* $\mathbf{v}$ and $\mathbf{k}$ becomes simply matrix multiplication of $\mathbf{V}$ with $\mathbf{k}$,

$$\mathbf{v} \times \mathbf{k} = \mathbf{V} \cdot \mathbf{k}. \tag{36}$$

Generating the skew-symmetric matrix of $\hat{\mathbf{v}}$ is a key step in our algorithm that rotates the magnetic susceptibility matrix $\boldsymbol{\chi}$ to become aligned with the normal vector of a mesh triangle. In addition, built into the algorithm is handling the contingency when $\theta \sim 0$ and $\sim\pi$. An important consideration is ensuring that all normal vectors point outwards from the RBC surface. This depends on the consistent choice of the edge vectors used to make the calculations. The *Mathematica* Notebook that incorporates all these features is given in the Supporting Information (available here).

2.11. Total Energy and Energy Difference. In summary, the integral in equation (22) is approximated by the weighted sum of the $\mathcal{N}$ triangles in the meshing of the RBC. Based on equations (28)–(30), the volume of the membrane increment is the product of the area of each mesh triangle, and the thickness of the membrane w that is constant across the RBC surface. Therefore,

$$U = -\sum_{i=1}^{\mathcal{N}}\left(\frac{\mathbf{1}}{2\mu_0}\boldsymbol{\chi}'_{\text{m},i}\,\mathbf{B}\right)\mathbf{B}\,w\,dA_i, \tag{37}$$

and, from equation (23),

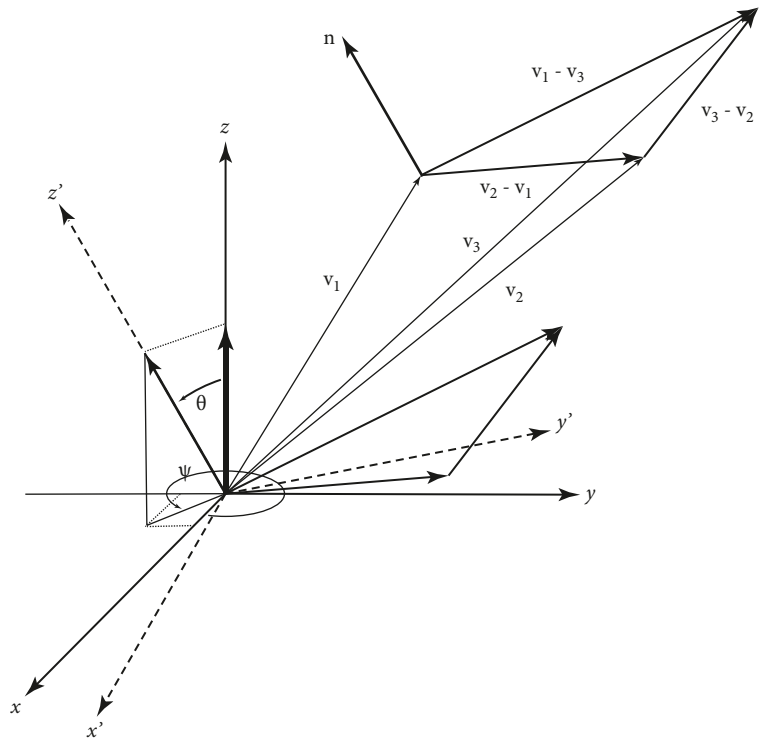

FIGURE 3: Cartesian coordinate system with *x*-, *y*-, and *z*-axes. The mesh triangle (upper right) is defined by the three *position vectors* (tails at the origin). The sides are defined by the *difference vectors* $\mathbf{v}_2$-$\mathbf{v}_1$, etc. The normal vector is **n**. The mesh triangle is, in effect, projected to the origin of the coordinate system by normalization (see the text). Then, we must rotate the normalized *z*-axis unit vector $\hat{\mathbf{k}}$ to align with $\hat{\mathbf{n}}$. The transformation matrix which does this is used to compute the magnetic susceptibility tensor in this mesh triangle frame of reference.

$$\mathbf{B} = B_{0,z}\begin{pmatrix} 0 \\ \sin\alpha \\ \cos\alpha \end{pmatrix}. \tag{38}$$

Note the factor of ½ in equation (37). This comes from the expression of the integral between 0 and $B_{0,z}$, as explained above (see the Supporting Information available here).

2.12. Reorientation Time. It is of considerable interest to estimate the reorientation time through 90° as a function of magnetic field strength. To model RBC rotational dynamics, we begin by estimating the torque on a *single* RBC. This rests on the definition of torque as the derivative of energy with respect to angular displacement. Hence,

$$\tau = -\frac{dU}{d\theta}, \tag{39}$$

and the finite difference counterpart is

$$\tau \sim -\frac{\Delta U}{\Delta\theta}. \tag{40}$$

Torque is analogous to force, which is the negative derivative of potential energy with respect to position. To estimate the orientation time under this torque, we require a drag coefficient ζ_r. This parameter characterizes how the rate of rotation of the body depends on torque. For ellipsoidal bodies, the torque is given by [33, 34]

$$\tau = \zeta_r \frac{d\theta}{dt}. \tag{41}$$

Equation (41) gives the torque required to rotate a sphere (a special case of an ellipsoid) at an angular velocity of $\omega = d\theta/dt$.

Hence, the time scale estimate is

$$t_{\text{align}} \sim \frac{\zeta_r\,\theta}{\tau}. \tag{42}$$

A simple expression for the ζ_r of the RBC shape has not been reported, but for a sphere it is [33, 34],

$$\zeta_r = 8\,\pi\,\eta\,r^3, \tag{43}$$

where η is the viscosity of the medium (in blood plasma, or another physiological medium, ~1.2 mPa s compared to 0.7 mPa *s* for pure water at 37°C) and *r* is the Stokes radius of the sphere. The mean volume of a human RBC is 86 fL [35] corresponding to a sphere of radius 2.7 μm. Therefore, $\zeta_r = 8\,\pi \times 1.2 \times 10^{-3} \times (2.7 \times 10^{-6})^3 = 5.93 \times 10^{-19}$ N m s.

3. Discussion of Calculations

Energies were obtained using a mesh of 780 surface triangles for an isolated RBC in plasma. When aligned with its disk planes parallel to a field of $\mathbf{B}_0 = 9.4$ T, the magnetic energy is calculated to be 1.28×10^{-16} J and 1.33×10^{-16} J when aligned perpendicular, with an energy difference of 4.70×10^{-18} J. For a finer mesh of 67,292 triangles, the

energies were 1.31×10^{-16} J and 1.28×10^{-16} J, respectively, with a difference of 4.82×10^{-18} J. Given the approximations inherent in the theoretical model, this difference is deemed to be "acceptable," suggesting that coarser meshes may be used routinely for computational efficiency without significantly compromising accuracy.

The energy difference (ΔU) can be contextualized by considering the thermal energy available to a particle/molecule given by $k_B T$, where k_B is Boltzmann's constant and T is the absolute temperature [34]. Hence, at the temperature of the human body, 37°C (310 K), $k_B T = 4.03 \times 10^{-21}$ J. Multiplying this value by Avogadro's number gives 2.6 kJ mol^{-1}. For comparison with other energies encountered in (bio)chemistry, typical bond energies are hydrogen bond: ~20 kJ mol^{-1} (~8 $k_B T$); ionic bond: ~20 kJ mol^{-1} (~12 $k_B T$); and covalent bond: ~400 kJ mol^{-1} (~160 $k_B T$). An energy difference of ~1200 $k_B T$ is well above the thermal energy and is equivalent to the energy of ~150 hydrogen bonds; it is modest if averaged over the volume of the RBC, but certainly sufficient to drive reorientation of a suspension of RBCs in an NMR magnet.

Using this energy difference, we can estimate the torque for $\Delta\theta = 1$ radian reorientation at 9.4 T field strength $\tau = 4.83 \times 10^{-18}$ Nm. We can then calculate the reorientation time of an RBC, approximating this to the reorientation time of a sphere of the same volume, for $\theta = \pi/2 = 1.57$ radians, and from equation (42), $t = (5.93 \times 10^{-19} \times 1.57)/4.82 \times 10^{-18} = 0.304$ s. In words, the reorientation time of an isolated RBC, from lying perpendicular to $\mathbf{B}_0$ to being aligned parallel, is ~300 ms.

Using the attached *Mathematica* Notebook (Supporting Information available here), we can calculate the timescale for the magnetic alignment of an isolated RBC under different experimental conditions. Figure 4(b) shows reorientation time t calculated using equation (42) and plotted *vs.* the magnitude of the magnetic field strength $\mathbf{B}_0$ and solution viscosities that might typically be encountered in suspensions of RBCs. In the regime of benchtop NMR spectrometers or typical MRI scanners, *i.e.*, $\mathbf{B}_0 < 3$ T, the reorientation time is predicted to be considerably longer, *e.g.*, at 1 T, the reorientation time is $t \simeq 27$ s, while at higher magnetic field strengths typical of superconducting NMR systems, *i.e.,* $\mathbf{B}_0 > 7$ T, the reorientation time is predicted to be less than 1 s. At $\mathbf{B}_0 = 18.8$ T, the reorientation time is $t \simeq 75$ ms—approximately three orders of magnitude faster than at 1 T.

The above calculations are valid for a single cell. However, the tendency for an ensemble of RBCs to realign in the magnetic field will depend on cell geometry as well as packing density/*Ht*. The drag coefficient for a biconcave disk will be greater than a sphere, and the drag coefficient will also depend on the viscosity of the medium, both leading to a slower reorientation time.

The viscosity of an RBC suspension is higher than that of plasma and depends on both *Ht* and plasma protein concentration and composition. In normal blood (*Ht* = 40%–50%), viscosity is typically 3–4 mPa s. At even higher *Ht* values as used in NMR experiments (*e.g.*, ~70%), viscosity may increase by an order of magnitude relative to normal blood (as also reported in polycythemia [36]), resulting in a drag coefficient (equation (43)) approximately tenfold greater. This, in turn, implies an alignment time on the order of ~3 s at 9.4 T due to the linear dependence of reorientation time on viscosity. In contrast, in extreme cases such as Waldenström macroglobulinemia with hyperviscosity syndrome, values can rise to ~20 mPa s owing to markedly elevated plasma protein levels [37].

The alignment of RBCs should also be viewed as a collective process; as one RBC begins to align, it can induce subtle displacements in its neighbors, promoting a *collective* reorientation event and hence speeding up the whole process. In other words, such a collective effect will accelerate the realignment response of the overall suspension. Philp previously reported a magnetic energy difference much smaller than our estimate [25]. In rationalizing the low value and the fact that the RBCs were known to align in $\mathbf{B}_0$, this was attributed to cooperative interactions within rouleaux, stacks of RBCs held together by surface charges on integral membrane proteins and proteins in the medium. However, our experimental RBC samples are typically washed in physiological saline, free of extraneous proteins, and under the light microscope, they show no evidence of rouleaux formation. These inferences can be avoided now that our new calculations reveal a much larger alignment energy based solely on the diamagnetic susceptibility of the cell membrane. The timescale for the reorientation of an RBC in a strong magnetic field is in accordance with experimental measurements from optical transmittance [2].

Finally, it is instructive to calculate the change in temperature when RBCs that are totally aligned across a homogeneous 9.4 T magnetic field line up with their disk planes parallel to it: Assume an *Ht* of 0.75 and cell volume of 86 fL, then there are $N = 8.72 \times 10^{12}$ RBC L^{-1}. The energy difference per RBC is $\Delta E = 1200\, k_B T$; $T = 310$ K; and $k_B = 1.380649 \times 10^{-23}$ J K^{-1}. This gives a total energy difference of

$$E_{\text{total}} = \Delta E \times N = 5.13 \times 10^{-18} \times 8.72 \times 10^{12} \approx 44.7 \text{ J}. \tag{44}$$

Suppose the sample is effectively 1 L of water (30% of the cells' volume is protein and lipid which from the point of view of heat capacity is like water); this has a specific heat capacity, C, of 4184 J kg^{-1} K^{-1}. Hence [38],

$$\Delta T = \frac{E_{\text{total}}}{C} = \frac{44.7}{4184} \approx 0.0107 \text{ K}. \tag{45}$$

This means there would be a temperature drop of 0.011 K when the cells reorientate.

Such changes may be experimentally detectable with microcalorimetry as they are vastly in excess of "thermal noise" in water at 310 K, which has a standard deviation of [38],

$$\sigma_T = \sqrt{\frac{k_B T^2}{C}}, \tag{46}$$

$$\sigma_T \approx 6.2 \times 10^{-9} \text{ K}. \tag{47}$$

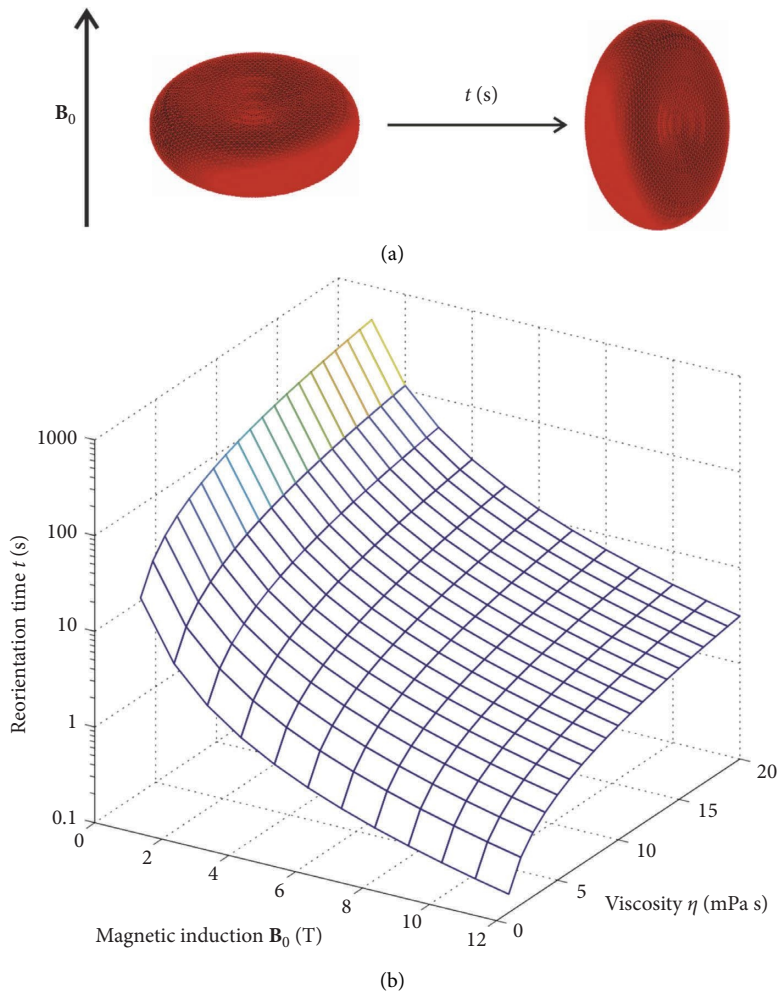

FIGURE 4: (a) Schematic reorientation of an RBC from lying perpendicular to the magnetic field $\mathbf{B}_0$ to parallel. (b) RBC reorientation time t (s) as a function of the magnitude of the magnetic induction $\mathbf{B}_0$ (T) of typical NMR spectrometers or MRI scanners and solution viscosity η (mPa s) typically encountered in suspensions of RBCs.

This is over 600 million times smaller than the temperature change caused by the RBC reorientation energy.

4. Conclusions

We have quantified the magnetic energy difference associated with the orientation of an RBC in a strong magnetic field, demonstrating that the alignment of its disk plane with $\mathbf{B}_0$ results in a significant energy difference, compared with the perpendicular orientation. For meshes of increasing refinement (from 780 to 67,292 surface triangles), the calculated energy difference (ΔU) remained consistent at $\sim 4.8 \times 10^{-18}$ J, confirming the robustness of the simulations and justifying the use of coarse meshes for computational efficiency. This energy difference is sufficient to drive subsecond reorientation dynamics of RBCs in strong magnetic fields.

Our calculations support the view that individual RBCs respond to the magnetic field independently, without requiring the presence of cooperative interactions to explain alignment, as previously postulated. This finding is highly relevant to a range of cell NMR experiments where alignment of the cells reintroduces residual anisotropic interactions; for example, residual dipolar or quadrupolar couplings.

Finally, our theoretical findings underscore the need for much more work in defining magnetic anisotropy of membrane components, and the behavior of whole membrane assemblies. This current work also highlights the role of geometry, anisotropic susceptibility, and viscous drag in determining the magneto-orientational behavior of RBCs; and the mathematical simulations set the stage for characterizing more complex suspensions, lipid bicelles, or dynamic magnetic field manipulations in future studies. The latter could employ a Monte Carlo method (*e.g.*, Ref. [39]) with avoidance criteria built into the algorithm.

Nomenclature

μ_0 magnetic permeability of free space
χ magnetic susceptibility

$\mathbf{B}_0$ uniform magnetic field (strictly, "magnetic induction")
$\mathbf{H}$ magnetic field strength
Ht hematocrit
$\mathbf{M}$ magnetization
RBC red blood cell
SI Standard International.

Data Availability Statement

The data that support the findings of this study are available on request from the corresponding author.

Conflicts of Interest

The authors declare no conflicts of interest.

Funding

This study was supported by the Australian Research Council, DP0100510, and Engineering and Physical Sciences Research Council, WT203148/Z/16/Z.

Acknowledgments

Chris Durrant and Denis Winch, Applied Mathematics, University of Sydney, are thanked for enlightening discussions, along with David Philp who carried out our initial theoretical work on this problem. The study was part of an Australian Research Council Grant DP0100510 to PWK. For ongoing NMR-related work, PWK thanks Ian Luck and Biswaranjan Mohanty of Sydney Analytical. TRE acknowledges support from the BHF Centre of Research Excellence (RE/18/2/34213) and the Centre of Excellence in Medical Engineering funded by the Wellcome Trust and EPSRC (WT 203148/Z/16/Z). SJE thanks Mark Crimmin and Lisa Haigh for their continuing support. *Note On The Use Of Artificial Intelligence*: Both Microsoft Copilot and ChatGPT were used as sounding boards for literature searching, mathematical and physical ideas, and text expression, but not as the final arbiters on any of these matters.

Supporting Information

Additional supporting information can be found online in the Supporting Information section. *(Supporting Information)*

This contains the *Mathematica* Notebook that represents the shape of an RBC using disk-cyclide coordinates and Cartesian coordinates and uses the latter to calculate the magnetic energy of an RBC at any orientation with respect to a uniform applied magnetic field $\mathbf{B}_0$.

References

[1] M. Murayama, "Orientation of Sickled Erythrocytes in a Magnetic Field," *Nature* 206, no. 4982 (1965): 420–422, https://doi.org/10.1038/206420a0.

[2] T. Higashi, A. Yamagishi, T. Takeuchi, et al., "Orientation of Erythrocytes in a Strong Static Magnetic Field," *Blood* 82, no. 4 (1993): 1328–1334, https://doi.org/10.1182/blood.v82.4.1328.bloodjournal8241328.

[3] T. Higashi, S. Sagawa, N. Ashida, and T. Takeuchi, "Orientation of glutaraldehyde-fixed Erythrocytes in Strong Static Magnetic Fields," *Bioelectromagnetics* 17, no. 4 (1996): 335–338, https://doi.org/10.1002/(sici)1521-186x(1996)17:4%3c335::aid-bem10%3e3.0.co;2-n.

[4] T. Suda and S. Uneo, "Magnetic Orientation of Red Blood Cell Membranes," *IEEE Transactions on Magnetics* 30, no. 6 (1994): 4713–4715, https://doi.org/10.1109/20.334198.

[5] T. Suda and S. Uneo, "On the Magnetic Orientation of Red Blood Cells: Behaviors in Whole Blood and Suspensions in Plasma," *1995 IEEE-EMBC and CMBC Theme 7: Instrumentation* (1997).

[6] P. W. Kuchel and B. E. Chapman, "Translational Diffusion of Haemoglobin in Human Erythrocytes and Haemolysates," *Journal of Magnetic Resonance* 94, no. 3 (1991): 574–580, https://doi.org/10.1016/0022-2364(91)90144-i.

[7] A. J. Lennon and P. W. Kuchel, "Enhancement of the "diffraction-like" Effect in NMR Diffusion Experiments," *Journal of Magnetic Resonance* 111, no. 2 (1994): 208–211, https://doi.org/10.1006/jmra.1994.1249.

[8] P. T. Callaghan, "Principles of Nuclear Magnetic Resonance Microscopy," *Oxfordian*, 492 (Oxford University Press, 1993).

[9] P. Kuchel, A. Coy, and P. Stilbs, "NMR "Diffusion-diffraction" of Water Revealing Alignment of Erythrocytes in a Magnetic Field and Their Dimensions and Membrane Transport Characteristics," *Magnetic Resonance in Medicine* 37, no. 5 (1997): 637–643, https://doi.org/10.1002/mrm.1910370502.

[10] P. W. Kuchel, T. R. Eykyn, and D. G. Regan, "Measurement of Compartment Size in *q*-space Experiments: Fourier Transform of the Second Derivative," *Magnetic Resonance in Medicine* 52, no. 4 (2004): 907–912, https://doi.org/10.1002/mrm.20219.

[11] A. M. Torres, R. J. Michniewicz, B. E. Chapman, G. A. Young, and P. W. Kuchel, "Characterisation of Erythrocyte Shapes and Sizes by NMR diffusion-diffraction of Water: Correlations With Electron Micrographs," *Magnetic Resonance Imaging* 16, no. 4 (1998): 423–434, https://doi.org/10.1016/s0730-725x(98)00005-8.

[12] P. W. Kuchel, C. J. Durrant, B. E. Chapman, P. S. Jarrett, and D. G. Regan, "Evidence of Red Cell Alignment in the Magnetic Field of an NMR Spectrometer Based on the Diffusion Tensor of Water," *Journal of Magnetic Resonance* 145, no. 2 (2000): 291–301, https://doi.org/10.1006/jmre.2000.2093.

[13] D. G. Regan and P. W. Kuchel, "Simulations of Molecular Diffusion in Lattices of Cells: Insights for NMR of Red Blood Cells," *Biophysical Journal* 83, no. 1 (2002): 161–171, https://doi.org/10.1016/s0006-3495(02)75158-8.

[14] E. Protopapas, P. Vafeas, and M. Hadjinicolaou, "A Mathematical Model for Studying the Red Blood Cell Magnetic Susceptibility," *Applied Numerical Mathematics* 208 (2025): 356–365, https://doi.org/10.1016/j.apnum.2024.05.014.

[15] G. Pagès and P. W. Kuchel, "NMR Methods for the Fast Recording of Diffusion," in *Diffusion Fundamentals II L'Aquila 2007*, ed. S. Brandini, et al. (2007), 52–68.

[16] G. Pagès, D. Szekely, and P. W. Kuchel, "Erythrocyte Shape Evolution Measured With Fast NMR diffusion-diffraction," *Journal of Magnetic Resonance Imaging* 28, no. 6 (2008): 1409–1416, https://doi.org/10.1002/jmri.21588.

[17] E. R. Dobbs, *Electricity and Magnetism* (London: Routledge & Kegan Paul, 1984).

[18] D. J. Griffiths, *Introduction to Electrodynamics* (Upper Saddle River, NJ: Prentice Hall, 1999).

[19] P. W. Kuchel, B. E. Chapman, W. A. Bubb, P. E. Hansen, C. J. Durrant, and M. P. Hertzberg, "Magnetic Susceptibility: Solutions, Emulsions, and Cells," *Concepts in Magnetic Resonance: Part A* 18, no. 1 (2003): 56–71, https://doi.org/10.1002/cmr.a.10066.

[20] R. C. Weast, *Handbook of Chemistry and Physics* (Boca Raton, FL: CRC Press, 1983).

[21] P. W. Kuchel and E. D. Fackerell, "Parametric-Equation Representation of Biconcave Erythrocytes," *Bulletin of Mathematical Biology* 61, no. 2 (1999): 209–220, https://doi.org/10.1006/bulm.1998.0064.

[22] P. W. Kuchel, C. D. Cox, D. Daners, D. Shishmarev, and P. Galvosas, "Surface Model of the Human Red Blood Cell Simulating Changes in Membrane Curvature Under Strain," *Scientific Reports* 11, no. 1 (2021): 13712–18pp, https://doi.org/10.1038/s41598-021-92699-7.

[23] P. Moon and D. E. Spencer, *Field Theory Handbook Including Coordinate Systems Differential Equations and Their Solutions. 2nd, Corrected 3rd Printing* (Berlin: Springer-Verlag, 1971).

[24] E. Evans and Y. C. Fung, "Improved Measurements of the Erythrocyte Geometry," *Microvascular Research* 4 (1972): 335–347, https://doi.org/10.1016/0026-2862(72)90069-6.

[25] D. J. Philp, "NMR Spectral Characteristics of Spin 1/2 and Spin >1/2 Nuclides in Erythrocyte Suspensions," in *School of Molecular and Microbial Biosciences* (PhD dissertation, New South Wales: University of Sydney, 2005).

[26] M. Babaei, I. C. Jones, K. Dayal, and M. S. Mauter, "Computing the Diamagnetic Susceptibility and Diamagnetic Anisotropy of Membrane Proteins From Structural Subunits," *Journal of Chemical Theory and Computation* 13, no. 6 (2017): 2945–2953, https://doi.org/10.1021/acs.jctc.6b01251.

[27] J. Seelig, "Deuterium Magnetic Resonance: Theory and Application to Lipid Membranes," *Quarterly Reviews of Biophysics* 10, no. 3 (1977): 353–418, https://doi.org/10.1017/s0033583500002948.

[28] J. Seelig, F. Borle, and T. A. Cross, "Magnetic Ordering of Phospholipid Membranes," *Biochimica et Biophysica Acta* 814, no. 1 (1985): 195–198, https://doi.org/10.1016/0005-2736(85)90437-7.

[29] L. Pauling, "The Diamagnetic Anisotropy of Aromatic Molecules," *Journal of Chemical Physics* 4, no. 10 (1936): 673–677, https://doi.org/10.1063/1.1749766.

[30] K. Lonsdale, "Diamagnetic Anisotropy of Organic Molecules," *Proceedings of the Royal Society A: Mathematical, Physical and Engineering Sciences* 171, no. 947 (1939): 541–568.

[31] H. Goldstein, *Classical Mechanics* (Reading MA: Addison-Wesley, 1980).

[32] S. Belongie, "Rodrigues' Rotation Formula," *MathWorld-A Wolfram Resource* 1 (2025): https://mathworld.wolfram.com/RodriguesRotationFormula.html.

[33] K. E. van Holde, *Physical Biochemistry* (Englewood Cliffs, NJ: Prentice-Hall, 1985).

[34] H. C. Berg, *Random Walks in Biology* (Princeton, NJ: Princeton University Press, 1993).

[35] J. V. Dacie and S. M. Lewis, *Practical Haematology* (Edinburgh: Churchill Livingstone, 1975).

[36] G. R. Cokelet, in *The Rheology of Human Blood*, ed. Y. C. Fung (Eaglewood Cliffs, NJ: Prentice-Hall, 1972).

[37] J. L. Fahey, W. F. Barth, and A. K. Solomon, "Serum Hyperviscosity Syndrome," *Journal of the American Medical Association* 192, no. 6 (1965): 464–467, https://doi.org/10.1001/jama.1965.03080190030008.

[38] H. B. Callen, *Thermodynamics and an Introduction to Thermostatistics* (New York, NY: Wiley, 1985).

[39] D. G. Regan and P. W. Kuchel, "Mean Residence Time of Molecules Diffusing in a Cell Bounded by a Semi-permeable Membrane: Monte Carlo Simulations and an Expression Relating Membrane Transition Probability to Permeability," *European Biophysics Journal* 29, no. 3 (2000): 221–227, https://doi.org/10.1007/s002490000081.